

See discussions, stats, and author profiles for this publication at: <https://www.researchgate.net/publication/272834284>

Functionalization of Transition Metal Dichalcogenides with Metallic Nanoparticles: Implications for Doping and Gas-Sensing

Article in Nano Letters · February 2015

DOI: 10.1021/nl504454u · Source: PubMed

CITATIONS

280

READS

465

8 authors, including:



Deblina Sarkar

Massachusetts Institute of Technology

44 PUBLICATIONS 4,679 CITATIONS

[SEE PROFILE](#)



Xuejun Xie

IMTmems

22 PUBLICATIONS 2,794 CITATIONS

[SEE PROFILE](#)



Jiahao Kang

Royole Corporation

58 PUBLICATIONS 5,374 CITATIONS

[SEE PROFILE](#)



Haojun Zhang

University of California, Santa Barbara

37 PUBLICATIONS 669 CITATIONS

[SEE PROFILE](#)

Some of the authors of this publication are also working on these related projects:



Project

Drug Research [View project](#)



Project

retromer [View project](#)

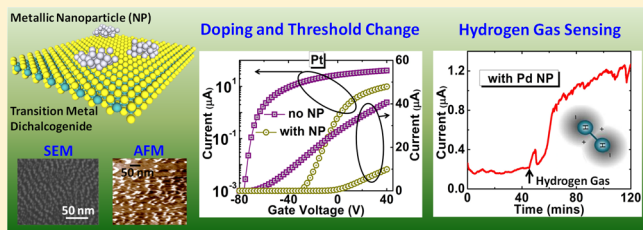
Functionalization of Transition Metal Dichalcogenides with Metallic Nanoparticles: Implications for Doping and Gas-Sensing

Deblina Sarkar,^{*,†} Xuejun Xie,[†] Jiahao Kang,[†] Haojun Zhang,[†] Wei Liu,[†] Jose Navarrete,[‡] Martin Moskovits,[‡] and Kaustav Banerjee^{*,†}

[†]Department of Electrical and Computer Engineering and [‡]Department of Chemistry and Biochemistry, University of California, Santa Barbara, Santa Barbara, California 93106, United States

Supporting Information

ABSTRACT: Transition metal dichalcogenides (TMDs), belonging to the class of two-dimensional (2D) layered materials, have instigated a lot of interest in diverse application fields due to their unique electrical, mechanical, magnetic, and optical properties. Tuning the electrical properties of TMDs through charge transfer or doping is necessary for various optoelectronic applications. This paper presents the experimental investigation of the doping effect on TMDs, mainly focusing on molybdenum disulfide (MoS_2), by metallic nanoparticles (NPs), exploring noble metals such as silver (Ag), palladium (Pd), and platinum (Pt) as well as the low workfunction metals such as scandium (Sc) and yttrium (Y) for the first time. The dependence of the doping behavior of MoS_2 on the metal workfunction is demonstrated and it is shown that Pt nanoparticles can lead to as large as 137 V shift in threshold voltage of a back-gated monolayered MoS_2 FET. Variation of the MoS_2 FET transfer curves with the increase in the dose of NPs as well as the effect of the number of MoS_2 layers on the doping characteristics are also discussed for the first time. Moreover, the doping effect on WSe_2 is studied with the first demonstration of p-type doping using Pt NPs. Apart from doping, the use of metallic NP functionalized TMDs for gas sensing application is also demonstrated.



KEYWORDS: 2D materials, dichalcogenides, doping, metallic nanoparticles, noble metals, MoS_2 , WSe_2

Recently, two-dimensional (2D) materials^{1–19} have attracted a lot of attention. While graphene¹ is the most widely known 2D material, transition metal dichalcogenides (TMDs)^{2–10} have also triggered a lot of interest. TMDs consist of vertically stacked layers held together by relatively weak van der Waals force and each layer is formed of covalently bonded transition metal and dichalcogenide atoms arranged in a hexagonal lattice. The weak interlayer bonding allows TMDs to be mechanically exfoliated from bulk to form atomically thin flakes, just as graphene can be exfoliated from bulk graphite. TMDs are highly versatile and combine excellent electronic, optical, mechanical, and magnetic properties, which make these materials potential candidates for variety of novel applications. While graphene suffers from lack of bandgap, the presence of bandgap in TMDs combined with excellent electrostatics not only make them attractive materials for highly scalable digital field-effect transistors (FETs)³ but also for designing ultra-sensitive FET-based biosensors.²⁰ These materials are also very attractive for optical applications because they can lead to strong light emission, as demonstrated in photoluminescence experiments.²¹ TMDs also offer valley polarization through optical pumping and hence are promising for the recently developed field of valleytronics.²² Moreover, the TMDs possess unique edge effects and magnetic properties.^{23,24} For example, the magnetic states of the MoS_2 zigzag nanoribbons are enhanced by H-saturation and are much stronger than those of

graphene.²³ These properties can be leveraged for novel spintronics applications.

For various applications including FETs and photovoltaics, it is necessary to tune the electronic properties of TMDs through modulation of the mobile charge concentrations or in other words, doping. Both p- and n-type doping can be achieved electrostatically^{25,26} by application of gate voltage but it requires extra electrodes (gates) that can increase power dissipation and increase area. Another way of doping is through substitution of the transition metal^{27,28} or the chalcogenide²⁹ of TMDs with appropriate elements. However, substitutional doping disturbs the structure of the TMDs through defect formation. Although physisorption^{6,30} of molecules can also lead to doping effect, they are unstable in nature. Solution-based functionalization of TMD flakes have also been reported to achieve doping,^{31–33} but the functionalization process is generally complicated and time-consuming. Plasma-based doping^{34,35} leads to formation of defects and significant reduction in mobility. Hence, exploration of efficient doping methodologies are required, which would be stable, easy to implement, and would not lead to significant defects in the TMDs. In case of WSe_2 , efficient n-type doping using

Received: November 19, 2014

Revised: February 27, 2015



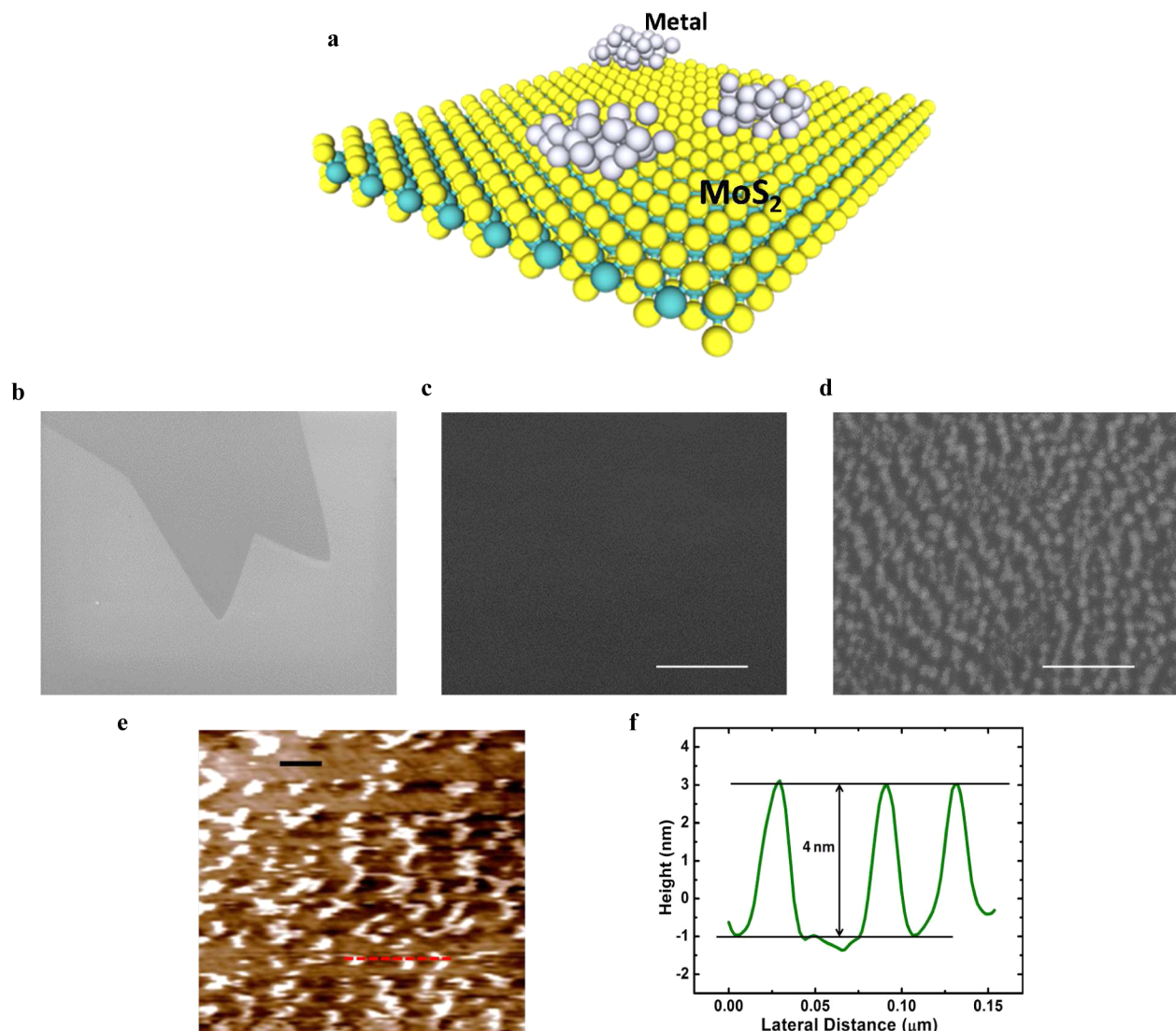


Figure 1. (a) Schematic diagram of an MoS₂ flake with metallic nanoparticles. (b) SEM micrograph of a MoS₂ flake on SiO₂/Si substrate. Magnified SEM image of the portion of the flake before any nanoparticle deposition, which is basically featureless as shown in (c) and after Pt NPs are deposited as shown in (d). Scale bar, 50 nm. The deposition rate used is 0.5 Å/s for 100 s. (e) AFM image showing NPs on MoS₂ flake. Scale bar (black line), 50 nm. (f) Height profile of the NPs along the red dotted line shown in (e).

potassium⁸ as well as silicon carbide thin films³⁶ have been shown. Cs₂CO₃³⁷ and 1,2 dichloroethane (DCE)³⁸ have been reported to lead to n-type doping of MoS₂. P-type doping of WSe₂ using NO_x chemisorption has been recently reported.³⁹ Also, p-type doping of MoS₂ using MoO₃ has been explored.⁴⁰ However, MoO₃ is very sensitive to the contaminants in the air leading to variations in its work function.⁴¹

The large surface-to-volume ratio offered by 2D TMD semiconductors offer unique opportunities for efficient surface functionalization/treatment to enable charge transfer to and from the atomically thin layered materials. Especially, incorporation of surface adatoms such as nanoparticles (NPs) of noble metals can be an effective way of doping 2D TMD materials, as these metals are resistant to environmental corrosion and oxidation. Moreover, functionalization using noble metallic NPs can also open up new avenues for gas sensing^{42–44} as well as biosensing⁴⁵ applications, as has been demonstrated in case of nanotubes/nanowires or graphene oxide. In this paper, we investigate the doping effect in TMDs caused by NPs of noble metals (Au, Ag, Pd, Pt) and show that

all these metallic NPs lead to p-type doping of MoS₂. The low work function metals such as scandium (Sc) and yttrium (Y) are also studied to demonstrate the relationship between metal work function and doping effect in MoS₂. While Sc leads to p-type doping, n-type doping can be obtained from Y. Moreover, it is shown that for MoS₂, Pt NPs can lead to as high as 2× higher p-type doping effect compared to that of the most commonly used Au NPs.^{46,47} While most experiments are performed using MoS₂, which is a typical representative of the TMD family, the doping effect of Pt NPs on WSe₂, another commonly used TMD material, is also explored. In addition, as a potential application of metallic NP incorporation on TMDs other than doping, detection of hydrogen gas using Pd functionalized MoS₂ is demonstrated in this work, because 2D materials are highly advantageous for gas sensing^{48–53} due to their high surface to volume ratio and sensitivity toward environmental changes.

Results and Discussion. The TMD flakes are obtained on 280 nm SiO₂/Si substrates using the micromechanical exfoliation technique, which is an efficient way for prototyping

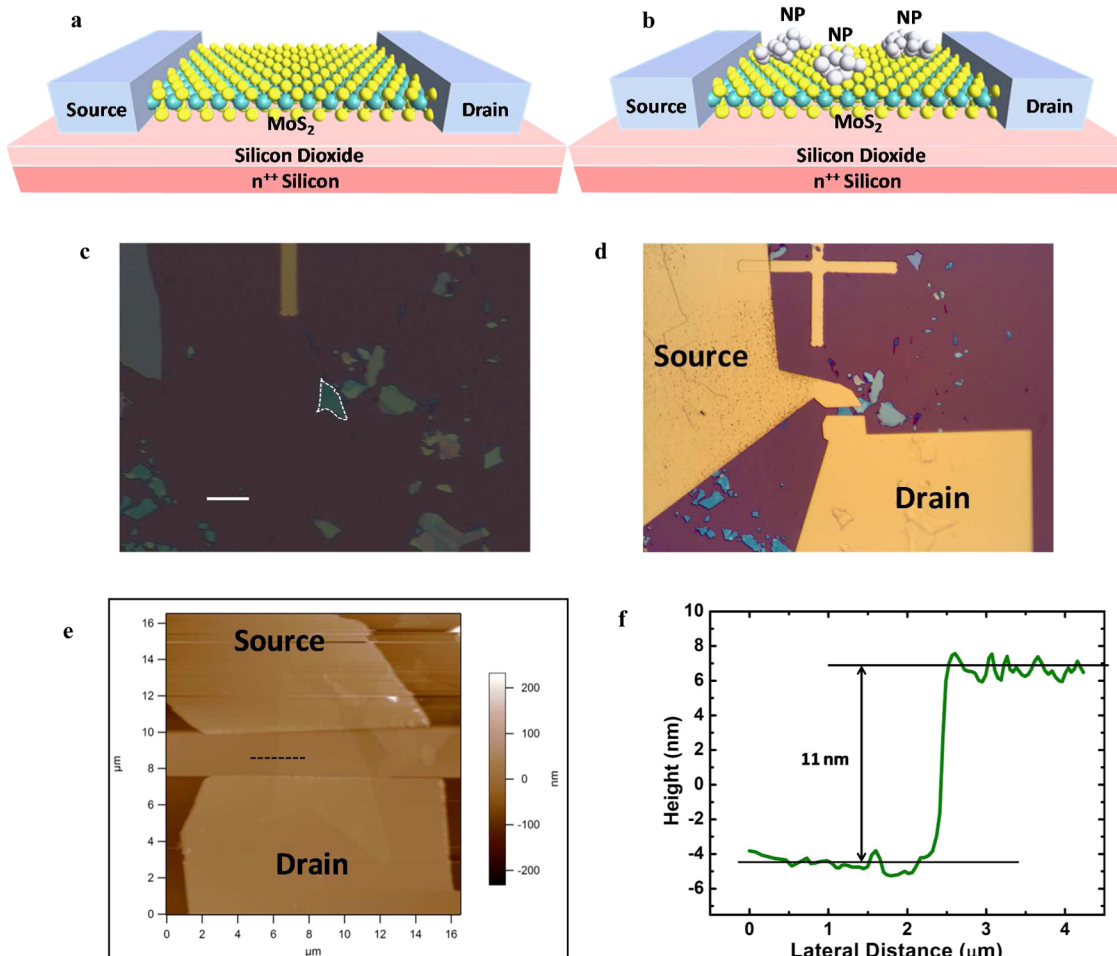


Figure 2. Schematic diagram of back-gated MoS₂ FET (a) without NPs and (b) with NPs. (c) Optical image of a MoS₂ flake (highlighted by white dotted line) mechanically exfoliated on 280 nm SiO₂ grown thermally on Si. Scale bar is 10 μm . (d) Optical image of the FET fabricated on the MoS₂ flake shown in (c). The source and drain regions were defined by e-beam lithography followed by e-beam deposition of 20 nm/100 nm Ni/Au. (e) AFM image of the MoS₂ FET. (f) Height profile of the MoS₂ flake along the black dotted line shown in (e).

experiments on various 2D materials.^{2–10} However, large area synthesis of MoS₂ is also made possible by the recent developments in liquid-scale exfoliation^{54,55} and chemical vapor deposition growth.^{56,57} The metallic nanoparticles are incorporated on the TMD sheet using electronic beam deposition. The schematic diagram of a MoS₂ flake with NPs is shown in Figure 1a. Figure 1b shows the scanning electron microscopy (SEM) image of a MoS₂ flake while Figure 1c,d shows the magnified images of a portion of the flake, without and with the NPs, respectively. The atomic force microscopy (AFM) characterization of the NPs is shown in Figure 1e,f.

Electrical measurements are an efficient way of characterizing the doping effect on semiconducting materials. Hence, field-effect transistors (schematic diagrams are shown in Figure 2a,b) are fabricated on the MoS₂ flakes (Figure 2c) with 20 nm/100 nm Ni/Au as source and drain metal contacts (Figure 2d). The underlying SiO₂ and the highly doped Si substrate are used as the gate dielectric and gate contact, respectively. The thickness of the flake is characterized using AFM (Figure 2e,f). To explore the effect of metallic NPs on MoS₂, the MoS₂ FET was measured first without the NPs and then the same device was measured again immediately after the deposition of NPs. Note that the metallic NPs do not form a continuous film and the current essentially flows through the MoS₂ channel. This is obvious because if a continuous metallic film would have

formed then current between the source and drain would essentially flow through the metallic film due to its lower resistance compared to semiconducting MoS₂, and therefore the current could not have been modulated by the gate. Figure 3a,b shows the $I_{\text{d}}-V_{\text{g}}$ and $I_{\text{d}}-V_{\text{d}}$ curves, respectively, before and after incorporation of the Ag NPs. The MoS₂ FET exhibits n-type transistor characteristics as the current increases with the increase in gate voltage. On incorporation of Ag NPs, the $I_{\text{d}}-V_{\text{g}}$ curve shifts toward the right compared to that without the NPs, indicating that more positive gate voltage is required to turn on the FET with NPs, implying p-type doping by the Ag NPs. The doping effect of other noble metallic NPs such as Au, Pd, and Pt are also explored as shown in Figure 3c–h. All these metals also lead to p-type doping as is clear from the shift of the $I_{\text{d}}-V_{\text{g}}$ curves. It is observed that Pt, which has the highest WF (about 5.9 eV) among these metals, results in the highest shift in $I_{\text{d}}-V_{\text{g}}$ curve and thereby, highest p-type doping. To investigate the effect of incorporation of metallic NPs with very low WF, experiments are carried out with scandium (Sc) with a WF of 3.5 eV and yttrium (Y) with a WF of 3.1 eV. Sc NPs are found to result in slight p-type doping as shown in Figure 4a. N-type doping can be obtained by using Y NPs as illustrated in Figure 4b,c. While in the case of multilayer MoS₂ FET, Y NPs can lead to only slight n-type doping (Figure 4b), the doping effect

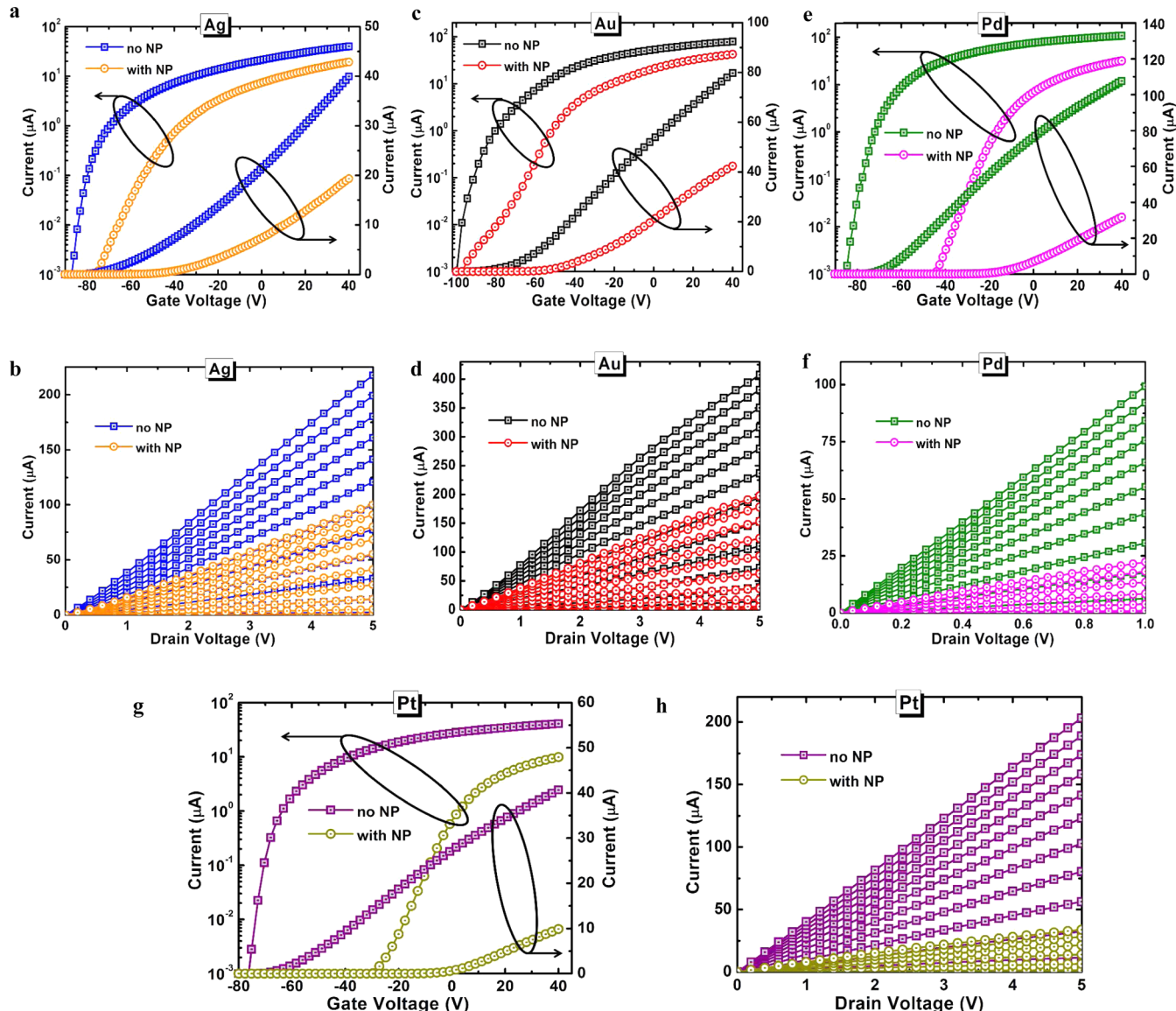


Figure 3. Drain current as a function of gate voltage ($I_d - V_g$) at $V_d = 1$ V, for MoS₂ FETs before and after incorporation of nanoparticles of (a) Ag, (c) Au, (e) Pd, and (g) Pt. The left axes show values in logarithmic scale while the right axes show values in linear scale. The drain current versus drain voltage ($I_d - V_d$) curves before and after incorporation of (b) Ag, (d) Au, (f) Pd, and (h) Pt where V_g is varied from -80 to 40 V in steps of 10 V, where the topmost curve is for V_g of 40 V. The thickness of the MoS₂ used in all the four cases is around 8 nm. All metals are deposited at the rate of 0.5 Å/s for 100 s. As can be observed from the $I_d - V_g$ curves, V_{TH} is negative for all cases since the MoS₂ is naturally n-doped. All the metallic NPs lead to p-type doping as is evident from the shift of the $I_d - V_g$ curves with NPs toward the right. Pt is observed to lead to the highest shift and hence to highest doping.

increased significantly when a monolayer MoS₂ is used (Figure 4c) as is evident from the higher shift of the $I_d - V_g$ curves.

The shift in threshold voltage (given by $\Delta V_{TH} = V_{TH,NP} - V_{TH}$ where V_{TH} and $V_{TH,NP}$ are the threshold voltages before and after the incorporation of NPs, respectively) as a function of WF of different metals is shown in Figure 5a. Since n-type doping means lower gate voltage is required to turn on the n-type devices and hence lower threshold voltage, the ΔV_{TH} is negative for Y as is clear from the figure. For the other metals, ΔV_{TH} is positive as they lead to p-type doping and with the increase in the metal WF, the ΔV_{TH} shows an increasing trend corroborating the increase in the p-type doping with the increase in the metal WF. The ratio of carrier concentrations with and without the NPs (given by $R_\xi = \xi_{NP}/\xi$ where ξ and ξ_{NP} are the carrier concentrations before and after incorpo-

ration of NPs, respectively) at a gate voltage of 40 V, is illustrated in Figure 5b. Because of the capacitive coupling of the gate, at positive gate voltage, 2D carrier (electron) density is formed at the semiconductor-dielectric interface. Since n-type doping leads to an increase in the effective carrier (electron) density, $R_\xi > 1$ for Y. However, in the case of the other metals, the effective carrier (electron) density is reduced due to the p-type doping, leading to $R_\xi < 1$. The higher the p-type doping, the lower will be the R_ξ . As shown in Figure 5b, R_ξ exhibits a decreasing trend with the increase in WF due to the increase in p-type doping. From Figure 5, it can be observed that Pt NPs can lead to a 2-fold higher doping effect compared to that of Au NPs, which has been commonly used to dope 2D materials.

As n-type doping can be obtained by using Y NPs, which however is not a noble metal, it is necessary to investigate its

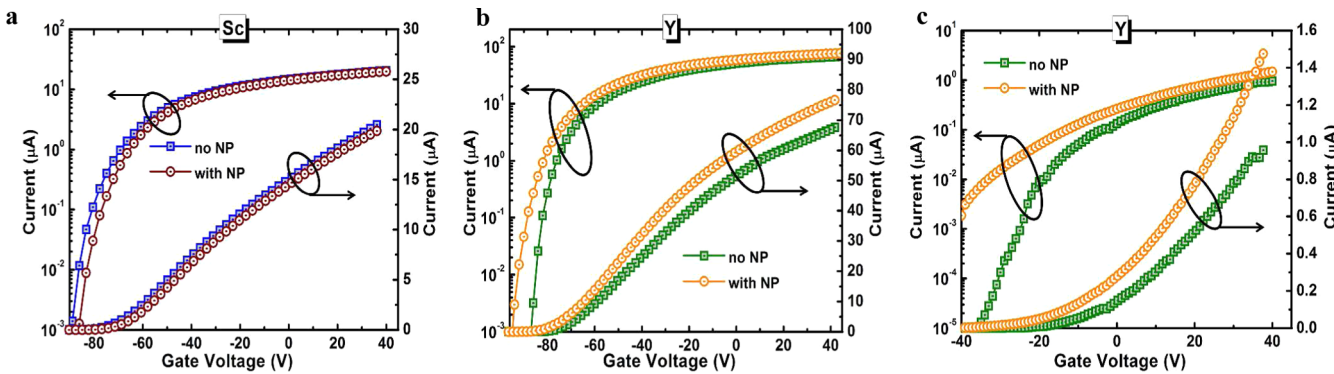


Figure 4. (a) Drain current as a function of gate voltage for MoS₂ FETs before and after incorporation of Sc nanoparticles. The left axis shows values in logarithmic scale while the right axis shows values in linear scale. The thickness of the MoS₂ used is around 8 nm. Sc NPs are found to shift the I_d – V_g curves slightly to the right indicating slight p-type doping. (b) The drain current versus gate voltage curves MoS₂ FET before and after incorporation of Y nanoparticles. Y NPs are found to shift the I_d – V_g curves slightly to the left indicating n-type doping. The thickness of the MoS₂ used is around 8 nm. (c) Significant n-type doping is obtained in case of a monolayer MoS₂ FET after incorporation of Y NPs. Note that, higher doping leads to decrease in gate control and hence, increase in subthreshold swing. Both Sc and Y are deposited at the rate of 0.5 Å/s for 100 s.

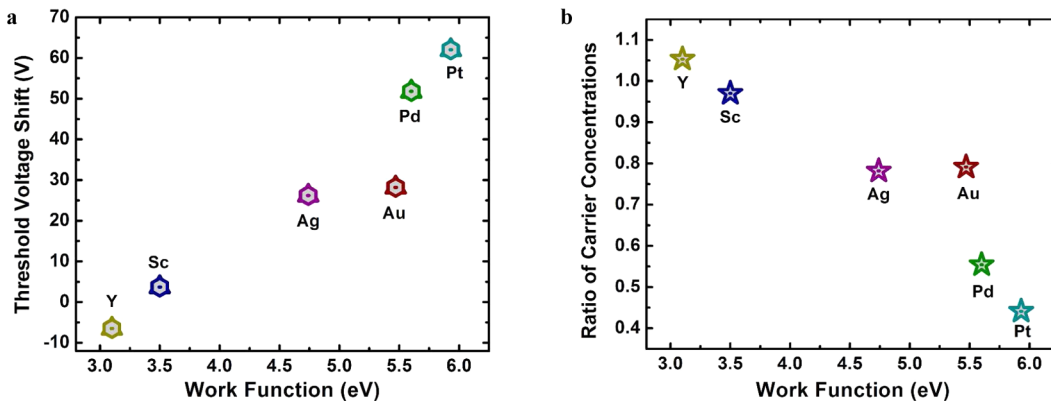


Figure 5. (a) Shift of ΔV_{TH} due to incorporation of NPs as a function of the WF of different metals. In case of Y, ΔV_{TH} is negative due to n-type doping. In case of all other metals, ΔV_{TH} is positive as they lead to p-type doping and an increasing trend is observed with increasing WF due to higher p-type doping by NPs of metals with higher WFs. (b) Ratio of carrier concentrations (R_c) after NPs incorporation to those before. R_c is higher than 1 for Y, as n-type doping by Y increases the effective carrier (electron) concentration. For all other metals, R_c is less than 1 and a decreasing trend is observed with increasing WF due to the decrease in the effective carrier (electron) concentrations with more p-type doping. The thickness of MoS₂ is similar in all the cases and is around 8 nm.

stability. Doping with Y NPs is found to be unstable and degraded on exposure to air due to the oxidation of Y (Supporting Information S1). On the other hand, noble metals are resistant to environmental attack and hence, lead to stable doping as shown in the case of Pt NPs (Supporting Information S1).

Because Pt NPs lead to the highest doping and at the same time is stable, the rest of the paper focuses on exploration of Pt NPs in more detail. Raman Spectroscopy is used to analyze the effect of Pt NPs. The Raman spectra excited by 632.8 nm line for a MoS₂ sheet before and after Pt NP incorporation is shown in Figure 6. For both the cases of with and without nanoparticles, apart from the E¹_{2g} and A_{1g} peaks, a peak is also visible around 455 cm⁻¹, which is typical for MoS₂ for excitation at 632.8 nm.⁵⁸ For MoS₂ with NPs, the features are shifted toward the right, indicating p-type doping.⁵⁹ Raman spectroscopy measurements were done at various points on the sample surface to take into account the effect of variations (Supporting Information S2). The clear shift in wavenumber to higher values for the case with NPs confirms p-type doping.⁵⁹ DFT simulations of the phonon spectra along with the physical

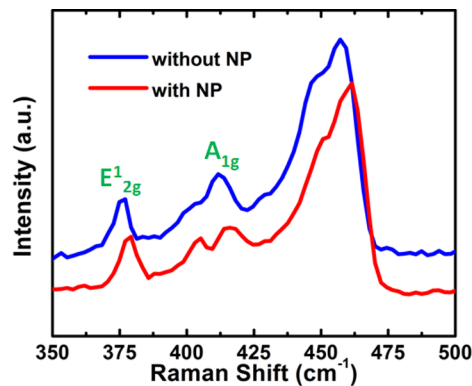


Figure 6. Raman spectra excited for a bulk MoS₂ sheet before and after incorporation of Pt NPs shown by blue and red lines, respectively. The red line is shifted toward the right compared to the blue line, indicating p-type doping by the Pt NPs.

explanation of the shift is presented in Supporting Information S3.

To better understand the doping effect of Pt NPs, ab initio density functional theory (DFT) calculations were performed.

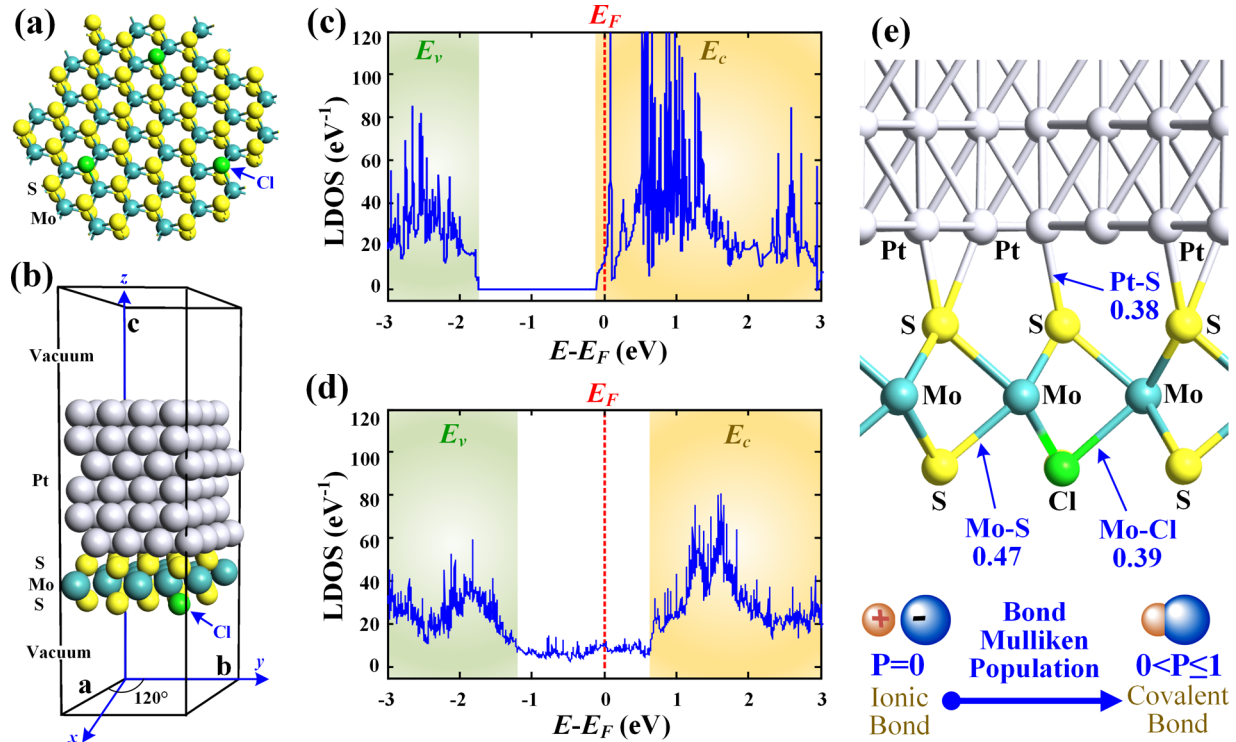


Figure 7. (a) The top view of MoS₂ with incorporated Cl atoms in order to simulate the n-type doping in MoS₂. (b) The schematic view of MoS₂–Cl–Pt system. (c) The local density of states diagram of MoS₂–Cl. The orange shaded region denotes the conduction band while the green shaded region denotes the valence band and the white region in between is the bandgap. The Fermi level, denoted by the red dashed line, lies in the conduction band clearly indicating an n-doped MoS₂. (d) After incorporation of Pt, the Fermi-level moves away from the conduction band indicating p-type doping by the Pt. (e) Schematic showing the Mulliken Population (P) for Mo–S bond (0.47), Mo–Cl bond (0.39), and Pt–S bond (0.38). $P = 0$ denotes ionic bond while $P > 0$ denote covalent bond. Thus, the positive value of P for Pt–S bond signifies that Pt forms covalent bond with the S of MoS₂.

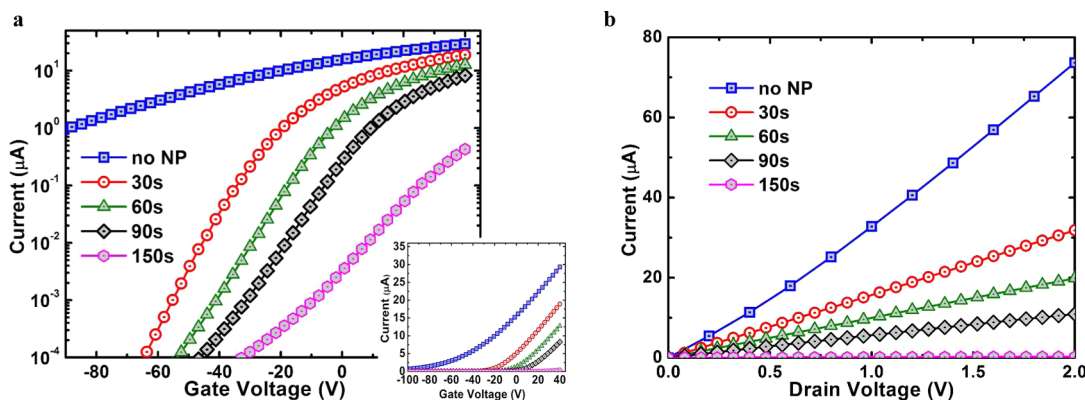


Figure 8. (a) Drain current as a function of gate voltage (I_d – V_g) curves for MoS₂ FET for different doses of Pt NPs. Thickness of MoS₂ used was around 8 nm. The I_d – V_g curve before the incorporation of Pt nanoparticles is shown by the blue curve. The MoS₂ flake used to fabricate this device is exfoliated from a bulk sample having higher intrinsic n-doping compared to that in previous figures, which allows observation of the effect of different Pt NP doses more prominently. The red, green, black, and magenta curves show I_d – V_g characteristics after deposition of Pt NPs at the rate of 0.2 Å/s for 30, 60, 90, and 150 s, respectively. The y-axis shows the values of current in logarithmic scale. The inset figure shows the curves in linear scale. The corresponding I_d – V_d curves at V_g = 40 V are shown in (b).

Because MoS₂ in general is naturally doped n-type, this n-type doping is simulated by using Cl atoms (as shown in Figure 7a), since from secondary ion mass spectrometry (SIMS), the samples were found to contain Cl. Because DFT only utilizes periodic boundary conditions with monocrystalline materials, metal–MoS₂–Cl system is modeled by a unit cell, which is periodic along lattice vector **a** and **b** and separated by vacuum in the **c** direction, as shown in Figure 7b. The unit cell contains a doped MoS₂ layer with Cl atoms as dopants, topped by a thin

film of Pt to emulate the Pt island. The mean absolute strain is 1.35% due to a slight lattice mismatch. All the atoms are allowed to relax.

It is important to note that the study of the metal–2D material interfaces (Figure 7b) requires careful treatment of the van der Waals (vdW) interaction between them. In order to reproduce such nonlocal dispersive force, which are important in weakly bonded systems, DFT-D2 approach⁶⁰ is used, where a semiempirical dispersion potential described by a simple

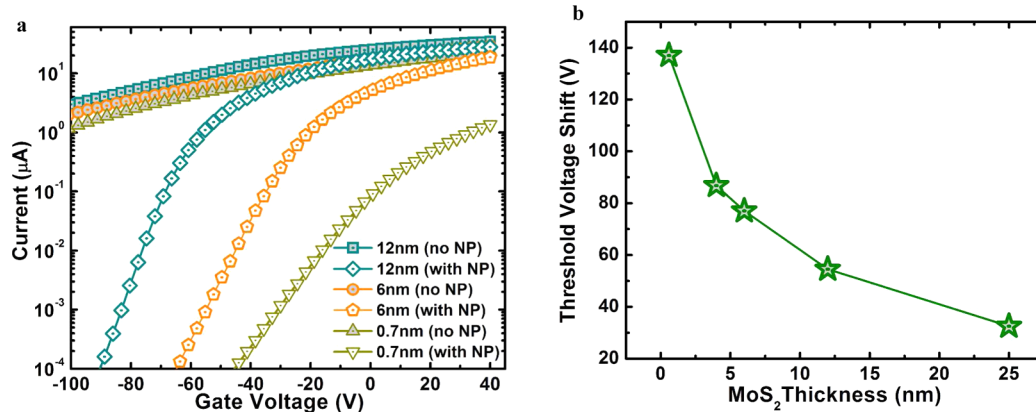


Figure 9. Effect of different thicknesses of MoS₂ on the doping characteristics. (a) I_d – V_g curves (with the current multiplied by their respective ratios of length to width) before and after incorporation of Pt NPs for different MoS₂ thicknesses. The thinner the MoS₂ is, higher is the shift in curve with NPs to the right compared to that without the NPs. (b) The threshold voltage shift decreases with increase in MoS₂ thickness indicating lower doping effect.

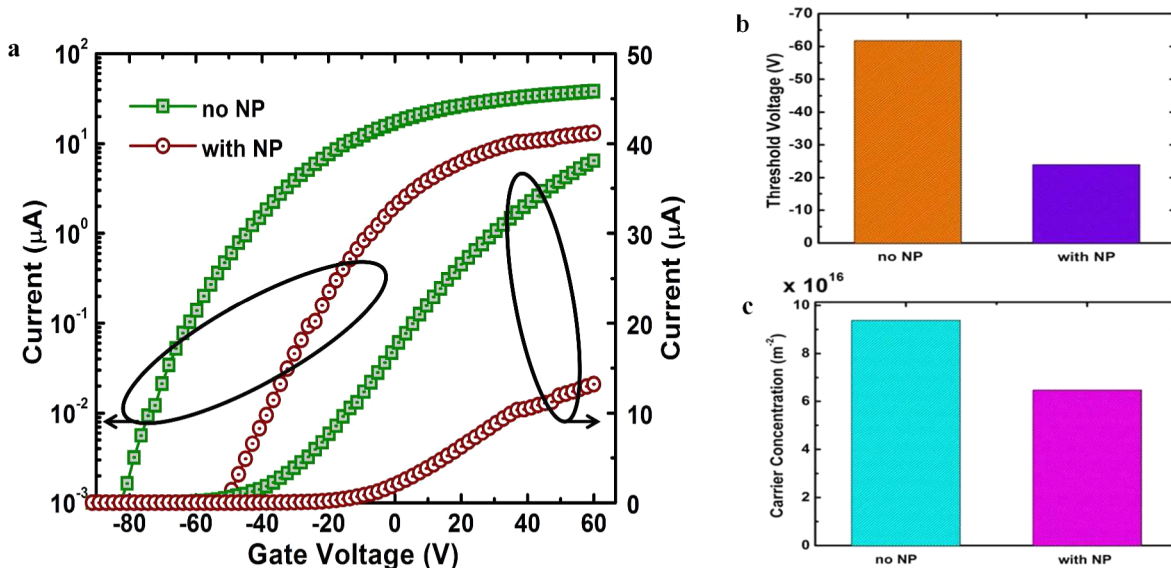


Figure 10. (a) Drain current as a function of gate voltage for *n*-type WSe₂ FETs before and after incorporation of Pt NPs. The left axis shows values in logarithmic scale while the right axis shows values in linear scale. The thickness of the WSe₂ used is around 9 nm. Pt is deposited at the rate of 0.5 Å/s for 100 s. Similar to the case for MoS₂, Pt NPs are found to shift the I_d – V_g curves to the right indicating p-type doping of WSe₂. (b) Threshold voltages before and after incorporation of Pt NPs showing shift toward more positive values in the presence of Pt NPs. (c) Carrier concentrations before and after incorporation of Pt NPs. Effective decrease in carrier (electron) concentration is observed due to the p-type doping by Pt NPs.

pairwise force field is added to the conventional Kohn–Sham DFT energy.

Local density approximation (LDA)⁶¹ is adopted for the exchange correlations, together with the double- ζ polarized basis set for expanding electronic density. The calculations are performed using Atomistix ToolKit (ATK).⁶² The $8 \times 8 \times 1$ k -points are sampled in the Brillouin zone (BZ). The temperature is set to be 300 K. The density mesh cutoff is 200 Ry and the maximum force is 0.05 eV/Å for geometry optimizations.

The density of state diagrams before and after the incorporation of Pt NPs are shown in Figure 7c,d, respectively. As is clear from the figures, after the incorporation of Pt NPs the Fermi level (denoted by the dashed line) shifts below the conduction band indicating p-type doping by the Pt NPs. Mulliken population analysis (Figure 7e) is also performed to understand the nature of bonding between Pt and MoS₂. Bond Mulliken population (P) represents the electronic charge distribution in a molecule and the nature of the molecular

orbitals for a pair of atoms.⁶³ The value of P varies from 0 to 1, where $P = 0$ and $0 < P \leq 1$ indicates ionic and covalent bonds, respectively. For covalent bonding, the numerical value of P indicates the strength of the bond. From Figure 7e it is clear that Pt forms covalent bonds with the sulfur of MoS₂ and the value of P for Pt–S bond is found to be 0.38.

The effect of different doses of Pt NPs on the MoS₂ FET is shown in Figure 8. First, the FET was measured without the NPs as shown by the blue curves in the I_d – V_g and I_d – V_d plots in Figure 8a,b, respectively. Then, the device was measured after deposition of Pt NPs at the rate of 0.2 Å/s for 30 s, as shown by the red curves. The same device was measured again after another 30 s (total 60 s) of deposition as shown by the green curves and yet again after another 30 s (total 90 s) of deposition as shown by the black curves and finally after another 60 s (total 150 s) of deposition as shown by the magenta curves, all at the same deposition rate. It is observed

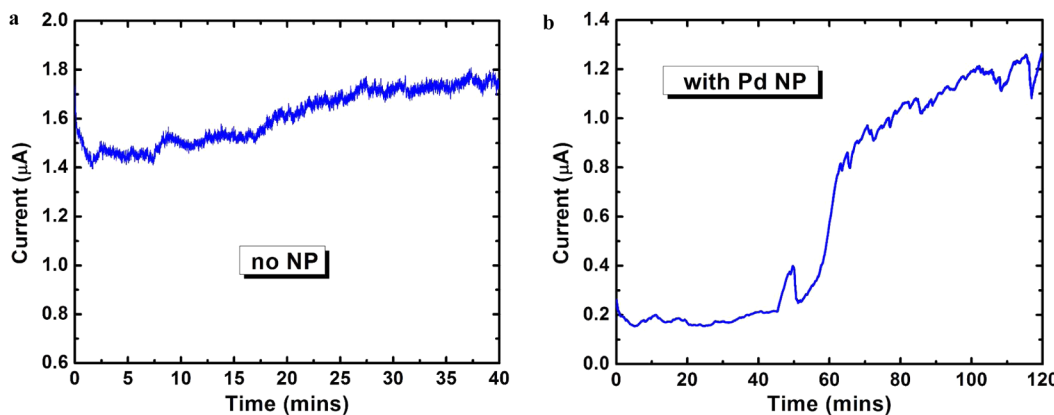


Figure 11. (a) Real-time measurement of current of MoS_2 FET without any NPs. Thickness of MoS_2 used was around 8 nm. Negligible change in current was observed when the device was exposed to hydrogen (from time = 20 min onwards). (b) Real-time measurement of current of the same MoS_2 FET after incorporation of Pd NPs. Current increases substantially upon exposure to hydrogen (3 ppm from time = 45 min onwards) from 0.2 μA to about 1 μA .

that by increasing the dose of Pt NPs in steps it is possible to gradually shift the transfer characteristics and dope the MoS_2 .

Next, the effect of MoS_2 thickness on the doping characteristics is investigated. For this purpose, MoS_2 flakes with different thicknesses are identified using optical contrast and the accurate thicknesses are measured using AFM. Subsequently, FETs are fabricated on the selected flakes. After initial measurements of the FET transfer characteristics, Pt NPs are deposited on the flakes at the same time, followed by another set of measurement with the NPs. To eliminate the effect of different lengths and widths of the FETs with different thicknesses, the currents of the devices are multiplied by their respective ratios of length to width and plotted in Figure 9a. It is observed that for almost similar levels of initial current, on incorporation of Pt NPs, the shift of the $I_d - V_g$ curve for the monolayered MoS_2 device is the highest (137 V) followed by those of the thicker MoS_2 devices. The threshold voltage shift is plotted as a function of the MoS_2 thickness in Figure 9b. It can be observed that the shift and hence the doping decreases with the increase in the thickness. This is because of the screening of the doping effect by the top MoS_2 layers.

Apart from MoS_2 , another TMD material most commonly used is WSe_2 .^{6–8} The doping effect of Pt NPs on WSe_2 is also explored by fabricating FETs and carrying out measurements in the same way as that of the MoS_2 experiments. The $I_d - V_g$ curves before and after incorporation of Pt NPs are shown in Figure 10a. p-type doping by the metallic NPs is evident from the shift of $I_d - V_g$ curve for FET with NPs toward the right. The threshold voltage and carrier concentration without and with the NPs are shown through the bar diagrams in Figure 10b,c, respectively, illustrating the increase in the threshold voltage and decrease in effective carrier (electron) concentration after NP incorporation.

Compared to the MoS_2 devices, the effective mobility (which includes the influence of contacts) of WSe_2 devices are found to be lower. This is because due to the lower electron affinity of WSe_2 , Ni forms higher Schottky barrier for n-type conduction with WSe_2 compared to MoS_2 . Mobility can be improved by choosing proper contact metals,^{64,65} which however is not the focus of this work. Effective mobility is calculated as $\mu = (L/W)dG/dV_g C_{\text{ox}}^{-1}$ in the linear region, where C_{ox} is the capacitance of the 280 nm thick bottom SiO_2 dielectric, G is the conductance, and L and W are the length and width of the

channel, respectively. For both MoS_2 and WSe_2 FETs, the mobility decreased slightly after incorporation of NPs. The mobility for WSe_2 before and after Pt NP incorporation are found to be 16.8 and $10.23 \text{ cm}^2 \text{ V}^{-1} \text{ s}^{-1}$, respectively, while those for MoS_2 FET are 32 and $26 \text{ cm}^2 \text{ V}^{-1} \text{ s}^{-1}$, respectively, where Pt is deposited at the rate of 0.5 \AA/s for 100 s .

It is clear from the above discussion that metallic NPs can be used to adjust the threshold voltage of TMD-based FETs that can be useful for digital applications. Apart from digital applications, metallic NPs can also be very useful for functionalizing the TMD surfaces for sensor applications. As an example, we configured an MoS_2 -based FET functionalized with Pd NPs as a gas sensor for sensing hydrogen gas. Pd can adsorb hydrogen, which leads to a change in its work function. As shown in the previous sections, the doping effect and hence the electrical characteristics of the MoS_2 FETs are dependent on the WF of the metallic NPs. Hence, change in the WF of Pd NPs due to adsorption of Hydrogen can be detected in real time through the change in current in a Pd NP functionalized MoS_2 FET. Figure 11a shows the current in a MoS_2 FET before the incorporation of any NPs. Negligible change in device current is observed upon exposure to hydrogen (3 ppm). The same device was then incorporated with Pd NPs and measured again in real time. In both the cases, the gate voltage was chosen to make the FET operate in the subthreshold region for obtaining maximum sensitivity.^{20,66–69} The current level was seen to increase substantially upon exposure to the same Hydrogen level as before. This is because adsorption of hydrogen led to decrease in the Pd WF,⁶⁸ thus decrease in the p-type doping and hence increase in the current level of the n-type MoS_2 transistor. Previously, sensitivity (defined as the ratio of change in conductivity/current to the initial conductivity/current) of much less than 1 was obtained at room temperature for 3 ppm of hydrogen gas exposure by using bulk MoS_2 .⁷⁰ In this work, for the same hydrogen concentration, sensitivity of about 5 is obtained at room temperature. This improvement is due to the use of few layer MoS_2 (8 nm thick) and biasing the device in subthreshold region.

Conclusion. In summary, the doping effect on MoS_2 by nanoparticles of different noble metals (Au, Ag, Pd, and Pt) is explored. Doping effect of Sc and Y with low WFs of 3.5 eV and 3.1 eV, respectively, are also investigated. It is observed that Au,

Ag, Pd, Pt, and Sc lead to p-type doping, which shows an increasing trend with increasing WF of the metals. Pt with the highest WF resulted in the highest doping, which is about 2-fold higher than that of most commonly used Au NPs. Pt NPs can lead to a shift in threshold voltage as high as 137 V in the case of monolayer MoS₂. While n-type doping can be obtained using Y, the doping effect is found not to be stable. It is also shown in this paper, that by stepwise increasing the dose of NPs, the doping intensity can be changed accordingly. It is also shown that doping effect increases with decreasing TMD thickness. Other than MoS₂, p-type doping of WSe₂ with Pt NPs is also explored. Finally, sensing of hydrogen gas using MoS₂ FET with incorporated Pd NPs is illustrated as a demonstration of another potential application of metallic NP functionalization.

Methods/Experimental. The MoS₂ flakes are mechanically exfoliated from bulk on 280 nm SiO₂ grown through thermal oxidation of degenerately n-doped Si substrates. SiO₂ (280 nm) can lead to sufficient contrast for optical detection of MoS₂/WSe₂ flakes. Optical microscopy, SEM, and AFM are used to characterize the flakes. For device fabrication, the source and drain regions are defined by e-beam lithography followed by electron beam (e-beam) deposition of 20 nm/100 nm Ni/Au. The devices are annealed in vacuum at 420 K for 20 min. The metallic NPs are incorporated using e-beam deposition tool.

■ ASSOCIATED CONTENT

Supporting Information

Stability analysis of Y and Pt NPs as dopants, Raman Spectroscopy data, and DFT simulations of the phonon spectra of intrinsic and p-doped MoS₂. This material is available free of charge via the Internet at <http://pubs.acs.org>.

■ AUTHOR INFORMATION

Corresponding Authors

*E-mail: deblina@ece.ucsb.edu (D.S.).

*E-mail: kaustav@ece.ucsb.edu (K.B.).

Author Contributions

The manuscript was written through contributions from all authors. All authors have given approval to the final version of the manuscript.

Notes

The authors declare no competing financial interest.

■ ACKNOWLEDGMENTS

This work was supported by the Air Force Office of Scientific Research, Arlington, VA, U.S.A., under Grant A9550-14-1-0268 (R18641). All process steps for device fabrication were carried out using the Nanostructure Cleanroom Facility at the California NanoSystems Institute and the Nanofabrication Facilities at UCSB - part of the National Nanotechnology Infrastructure Network. The authors made extensive use of the MRL Central Facilities at UCSB, which are supported by the MRSEC Program of the NSF (under Award No. DMR 1121053), a member of the NSF-funded Materials Research Facilities Network (www.mrfn.org).

■ REFERENCES

- (1) Geim, A. K.; Novoselov, K. S. The Rise of Graphene. *Nat. Mater.* 2007, 6, 183–192.
- (2) Novoselov, K. S.; Jiang, D.; Schedin, F.; Booth, T. J.; Khotkevich, V. V.; Morozov, S. V.; Geim, A. K. Two-Dimensional Atomic Crystals. *Proc. Natl. Acad. Sci. U.S.A.* 2005, 102, 10451–10453.
- (3) Radisavljevic, B.; Radenovic, A.; Brivio, J.; Giacometti, V.; Kis, A. Single-Layer MoS₂ Transistors. *Nat. Nanotechnol.* 2011, 6, 147–150.
- (4) Mak, K. F.; Lee, C.; Hone, J.; Shan, J.; Heinz, T. F. Atomically Thin MoS₂: A New Direct-Gap Semiconductor. *Phys. Rev. Lett.* 2010, 105, 136805.
- (5) Kim, S.; Konar, A.; Hwang, W.-S.; Lee, J. H.; Lee, J.; Yang, J.; Jung, C.; Kim, H.; Yoo, J.-B.; Choi, J.-Y.; et al. High-Mobility and Low-Power Thin-Film Transistors Based on Multilayer MoS₂ Crystals. *Nat. Commun.* 2012, 3, 1011.
- (6) Fang, H.; Chuang, S.; Chang, T. C.; Takei, K.; Takahashi, T.; Javey, A. High-Performance Single-Layered WSe₂ P-FETs with Chemically Doped Contacts. *Nano Lett.* 2012, 12, 3788.
- (7) Liu, W.; Kang, J.; Sarkar, D.; Khatami, Y.; Jena, D.; Banerjee, K. Role of Metal Contacts in Designing High-Performance Monolayer N-Type WSe₂ Field Effect Transistors. *Nano Lett.* 2013, 13, 1983–1990.
- (8) Fang, H.; Tosun, M.; Seol, G.; Chang, T. C.; Takei, K.; Guo, J.; Javey, A. Degenerate N-Doping of Few-Layer Transition Metal Dichalcogenides by Potassium. *Nano Lett.* 2013, 13, 1991–1995.
- (9) Liu, W.; Kang, J.; Cao, W.; Sarkar, D.; Khatami, Y.; Jena, D.; Banerjee, K. High-Performance Few-Layer-MoS₂ Field-Effect-Transistor with Record Low Contact-Resistance. *IEEE Int. Electron Devices Meet.* 2013, 499–502.
- (10) Xie, X.; Sarkar, D.; Liu, W.; Kang, J.; Marinov, O.; Deen, M. J.; Banerjee, K. Low-Frequency Noise in Bilayer MoS₂ Transistor. *ACS Nano* 2014, 8, 5633–5640.
- (11) Kang, J.; Cao, W.; Xie, X.; Sarkar, D.; Liu, W.; Banerjee, K. Graphene and beyond-Graphene 2D Crystals for next-Generation Green Electronics. *Proc. SPIE 9083, Micro-Nanotechnol. Sensors, Syst. Appl. VI* 2014, 908305.
- (12) Cao, W.; Kang, J.; Liu, W.; Khatami, Y.; Sarkar, D.; Banerjee, K. 2D Electronics: Graphene and beyond. *Proc. Eur. Solid-State Device Res. Conf.* 2013, 37–44.
- (13) Sarkar, D.; Xu, C.; Li, H.; Banerjee, K. High-Frequency Behavior of Graphene-Based Interconnects — Part I: Impedance Modeling. *IEEE Trans. Electron Devices* 2011, 58, 843–852.
- (14) Sarkar, D.; Xu, C.; Li, H.; Banerjee, K. High-Frequency Behavior of Graphene-Based Interconnects — Part II: Impedance Analysis and Implications for Inductor Design. *IEEE Trans. Electron Devices* 2011, 58, 853–859.
- (15) Sarkar, D.; Xu, C.; Li, H.; Banerjee, K. AC Conductance Modeling and Analysis of Graphene Nanoribbon Interconnects. *IEEE Int. Interconnect Technol. Conf.* 2010, 1–3.
- (16) Sarkar, D.; Krall, M.; Banerjee, K. Electron-Hole Duality during Band-to-Band Tunneling Process in Graphene-Nanoribbon Tunnel-Field-Effect-Transistors. *Appl. Phys. Lett.* 2010, 97, 263109.
- (17) Kang, J.; Sarkar, D.; Khatami, Y.; Banerjee, K. Proposal for All-Graphene Monolithic Logic Circuits. *Appl. Phys. Lett.* 2013, 103, 083113.
- (18) Liu, W.; Kraemer, S.; Sarkar, D.; Li, H.; Ajayan, P. M.; Banerjee, K. Controllable and Rapid Synthesis of High-Quality and Large-Area Bernal Stacked Bilayer Graphene Using Chemical Vapor Deposition. *Chem. Mater.* 2014, 26, 907–915.
- (19) Ye, P. D.; Liu, H.; Neal, A. T.; Zhu, Z.; Luo, Z.; Xu, X.; Engineering, C.; Lafayette, W.; States, U.; Lansing, E.; et al. Phosphorene: An Unexplored 2D Semiconductor with a High Hole Mobility. *ACS Nano* 2014, 4033–4041.
- (20) Sarkar, D.; Liu, W.; Xie, X.; Anselmo, A. C.; Mitragotri, S.; Banerjee, K. MoS₂ Field-Effect Transistor for Next-Generation Label-Free Biosensors. *ACS Nano* 2014, 8, 3992–4003.
- (21) Wang, Q. H.; Kalantar-Zadeh, K.; Kis, A.; Coleman, J. N.; Strano, M. S. Electronics and Optoelectronics of Two-Dimensional Transition Metal Dichalcogenides. *Nat. Nanotechnol.* 2012, 7, 699–712.
- (22) Zeng, H.; Dai, J.; Yao, W.; Xiao, D.; Cui, X. Valley Polarization in MoS₂ Monolayers by Optical Pumping. *Nat. Nanotechnol.* 2012, 7, 490–493.

- (23) Pan, H.; Zhang, Y.-W. Edge-Dependent Structural, Electronic and Magnetic Properties of MoS₂ Nanoribbons. *J. Mater. Chem.* **2012**, *22*, 7280.
- (24) Neal, A. T.; Liu, H.; Gu, J.; Ye, P. D. Magneto-Transport in MoS₂: Phase Coherence, Spin-Orbit Scattering, and the Hall Factor. *ACS Nano* **2013**, *7*, 7077–7082.
- (25) Yuan, H. T.; Toh, M.; Morimoto, K.; Tan, W.; Wei, F.; Shimotani, H.; Kloc, C.; Iwasa, Y. Liquid-Gated Electric-Double-Layer Transistor on Layered Metal Dichalcogenide, SnS₂. *Appl. Phys. Lett.* **2011**, *98*, 012102.
- (26) Pu, J.; Yomogida, Y.; Liu, K.-K.; Li, L.-J.; Iwasa, Y.; Takenobu, T. Highly Flexible MoS₂ Thin-Film Transistors with Ion Gel Dielectrics. *Nano Lett.* **2012**, *12*, 4013–4017.
- (27) Fedorov, V. E.; Naumov, N. G.; Lavrov, A. N.; Tarasenko, M. S.; Artemkina, S. B.; Romanenko, A. I. Tuning Electronic Properties of Molybdenum Disulfide by a Substitution in Metal Sublattice. In *36th IEEE International Convention on Information and Communication Technology Electronics and Microelectronics (MIPRO)*; May 20–24 2013, Opatija, Croatia; IEEE: Bellingham, WA, 2013; pp 11–14.
- (28) Laskar, M. R.; Nath, D. N.; Ma, L.; Lee, E. W.; Lee, C. H.; Kent, T.; Yang, Z.; Mishra, R.; Roldan, M. A.; Idrobo, J.-C.; et al. P-Type Doping of MoS₂ Thin Films Using Nb. *Appl. Phys. Lett.* **2014**, *104*, 092104.
- (29) Sun, Q.-Q.; Li, Y.-J.; He, J.-L.; Yang, W.; Zhou, P.; Lu, H.-L.; Ding, S.-J.; Wei Zhang, D. The Physics and Backward Diode Behavior of Heavily Doped Single Layer MoS₂ Based P-N Junctions. *Appl. Phys. Lett.* **2013**, *102*, 093104.
- (30) Tongay, S.; Zhou, J.; Ataca, C.; Liu, J.; Kang, J. S.; Matthews, T. S.; You, L.; Li, J.; Grossman, J. C.; Wu, J. Broad-Range Modulation of Light Emission in Two-Dimensional Semiconductors by Molecular Physisorption Gating. *Nano Lett.* **2013**, *13*, 2831–2836.
- (31) Li, Y.; Xu, C.; Hu, P.; Zhen, L. Carrier Control of MoS₂ Nanoflakes by Functional Self-Assembled Monolayers. *ACS Nano* **2013**, *7*, 7795–7804.
- (32) Du, Y.; Liu, H.; Neal, A. T.; Si, M.; Ye, P. D. Molecular Doping of Multilayer MoS₂ Field-Effect Transistors: Reduction in Sheet and Contact Resistances. *IEEE Electron Device Lett.* **2013**, *34*, 1328–1330.
- (33) Mouris, S.; Miyauchi, Y.; Matsuda, K. Tunable Photoluminescence of Monolayer MoS₂ via Chemical Doping. *Nano Lett.* **2013**, *13*, 5944–5948.
- (34) Chen, M.; Nam, H.; Wi, S.; Ji, L.; Ren, X.; Bian, L.; Lu, S.; Liang, X. Stable Few-Layer MoS₂ Rectifying Diodes Formed by Plasma-Assisted Doping. *Appl. Phys. Lett.* **2013**, *103*, 142110.
- (35) Wi, S.; Kim, H.; Chen, M.; Nam, H.; Guo, L. J.; Meyhofer, E.; Liang, X. Enhancement of Photovoltaic Response in Multilayer MoS₂ Induced by Plasma Doping. *ACS Nano* **2014**, *8*, 5270–5281.
- (36) Chen, K.; Kiriya, D.; Hettick, M.; Tosun, M.; Ha, T.-J.; Madhvapathy, S. R.; Desai, S.; Sachid, A.; Javey, A. Air Stable N-Doping of WSe₂ by Silicon Nitride Thin Films with Tunable Fixed Charge Density. *APL Mater.* **2014**, *2*, 092504.
- (37) Lin, J. D.; Han, C.; Wang, F.; Wang, R.; Xiang, D.; Qin, S.; Zhang, X.-A.; Wang, L.; Zhang, H.; Wee, A. T. S.; et al. Electron-Doping-Enhanced Trion Formation in Monolayer Molybdenum Disulfide Functionalized with Cesium Carbonate. *ACS Nano* **2014**, *8*, 5323–5329.
- (38) Yang, L.; Majumdar, K.; Du, Y.; Liu, H.; Wu, H.; Hatzistergos, M.; Hung, P. Y.; Tieckelmann, R.; Tsai, W.; Hobbs, C.; et al. High-Performance MoS₂ Field-Effect Transistors Enabled by Chloride Doping: Record Low Contact Resistance (0.5 K Ω·μm) and Record High Drain Current (460 μA/μm). *IEEE Symp. VLSI Technol.* **2014**, 1–2.
- (39) Zhao, P.; Kiriya, D.; Azcatl, A.; Zhang, C.; Tosun, M.; Liu, Y.; Hettick, M.; Kang, J. S.; McDonnell, S.; et al. Air Stable P-Doping of WSe₂ by Covalent Functionalization. *ACS Nano* **2014**, *8*, 10808–10814.
- (40) Lin, J.; Zhong, J.; Zhong, S.; Li, H.; Zhang, H.; Chen, W. Modulating Electronic Transport Properties of MoS₂ Field Effect Transistor by Surface Overlays. *Appl. Phys. Lett.* **2013**, *103*, 063109.
- (41) Cattin, L.; Morsli, M.; Bernède, J. Improvement in the Lifetime of Planar Organic Photovoltaic Cells through the Introduction of MoO₃ into Their Cathode Buffer Layers. *Electronics* **2014**, *3*, 122–131.
- (42) Mubeen, S.; Zhang, T.; Yoo, B.; Deshusses, M. A.; Myung, N. V. Palladium Nanoparticles Decorated Single-Walled Carbon Nanotube Hydrogen Sensor. *J. Phys. Chem. C* **2007**, *111*, 6321–6327.
- (43) Johnson, J. L.; Behnam, A.; Pearton, S. J.; Ural, A. Hydrogen Sensing Using Pd-Functionalized Multi-Layer Graphene Nanoribbon Networks. *Adv. Mater.* **2010**, *22*, 4877–4880.
- (44) Zhang, Y.; Xu, J.; Xu, P.; Zhu, Y.; Chen, X.; Yu, W. Decoration of ZnO Nanowires with Pt Nanoparticles and Their Improved Gas Sensing and Photocatalytic Performance. *Nanotechnology* **2010**, *21*, 285501.
- (45) Mao, S.; Lu, G.; Yu, K.; Bo, Z.; Chen, J. Specific Protein Detection Using Thermally Reduced Graphene Oxide Sheet Decorated with Gold Nanoparticle-Antibody Conjugates. *Adv. Mater.* **2010**, *22*, 3521–3526.
- (46) Sreeprasad, T. S.; Nguyen, P.; Kim, N.; Berry, V. Controlled, Defect-Guided, Metal-Nanoparticle Incorporation onto MoS₂ via Chemical and Microwave Routes: Electrical, Thermal, and Structural Properties. *Nano Lett.* **2013**, *13*, 4434–4441.
- (47) Shi, Y.; Huang, J.-K.; Jin, L.; Hsu, Y.-T.; Yu, S. F.; Li, L.-J.; Yang, H. Y. Selective Decoration of Au Nanoparticles on Monolayer MoS₂ Single Crystals. *Sci. Rep.* **2013**, *3*, 1839.
- (48) Li, H.; Yin, Z.; He, Q.; Li, H.; Huang, X.; Lu, G.; Fam, D. W. H.; Tok, A. I. Y.; Zhang, Q.; Zhang, H. Fabrication of Single- and Multilayer MoS₂ Film-Based Field-Effect Transistors for Sensing NO at Room Temperature. *Small* **2012**, *8*, 63–67.
- (49) Late, D. J.; Liu, B.; Matte, H. S. S. R.; Dravid, V. P.; Rao, C. N. R. Hysteresis in Single-Layer MoS₂ Field. *ACS Nano* **2012**, *6*, 5635–5641.
- (50) Rumyantsev, S.; Liu, G.; Shur, M. S.; Potyrailo, R. A.; Balandin, A. A. Selective Gas Sensing with a Single Pristine Graphene Transistor. *Nano Lett.* **2012**, *12*, 2294–2298.
- (51) Perkins, F. K.; Friedman, A. L.; Cobas, E.; Campbell, P. M.; Jernigan, G. G.; Jonker, B. T. Chemical Vapor Sensing with Monolayer MoS₂. *Nano Lett.* **2013**, *13*, 668–673.
- (52) Zhang, S.-L.; Choi, H.-H.; Yue, H.-Y.; Yang, W.-C. Controlled Exfoliation of Molybdenum Disulfide for Developing Thin Film Humidity Sensor. *Curr. Appl. Phys.* **2014**, *14*, 264–268.
- (53) Samnakay, R.; Jiang, C.; Rumyantsev, S. L.; Shur, M. S. Selective Chemical Vapor Sensing with MoS₂ Thin-Film Transistors: Comparison with Graphene Devices. 2014, arxiv1411.5393, pp 1–17.
- (54) Coleman, J. N.; Lotya, M.; O'Neill, A.; Bergin, S. D.; King, P. J.; Khan, U.; Young, K.; Gaucher, A.; De, S.; Smith, R. J.; et al. Two-Dimensional Nanosheets Produced by Liquid Exfoliation of Layered Materials. *Science* **2011**, *331*, 568–571.
- (55) Smith, R. J.; King, P. J.; Lotya, M.; Wirtz, C.; Khan, U.; De, S.; O'Neill, A.; Duesberg, G. S.; Grunlan, J. C.; Moriarty, G.; et al. Large-Scale Exfoliation of Inorganic Layered Compounds in Aqueous Surfactant Solutions. *Adv. Mater.* **2011**, *23*, 3944–3948.
- (56) Liu, K.-K.; Zhang, W.; Lee, Y.-H.; Lin, Y.-C.; Chang, M.-T.; Su, C.-Y.; Chang, C.-S.; Li, H.; Shi, Y.; Zhang, H.; et al. Growth of Large-Area and Highly Crystalline MoS₂ Thin Layers on Insulating Substrates. *Nano Lett.* **2012**, *12*, 1538–1544.
- (57) Zhan, Y.; Liu, Z.; Najmaei, S.; Ajayan, P. M.; Lou, J. Large-Area Vapor-Phase Growth and Characterization of MoS₂ Atomic Layers on a SiO₂ Substrate. *Small* **2012**, *8*, 966–971.
- (58) Li, H.; Zhang, Q.; Yap, C. C. R.; Tay, B. K.; Edwin, T. H. T.; Olivier, A.; Baillargeat, D. From Bulk to Monolayer MoS₂: Evolution of Raman Scattering. *Adv. Funct. Mater.* **2012**, *22*, 1385–1390.
- (59) Chakraborty, B.; Bera, A.; Muthu, D. V. S.; Bhowmick, S.; Waghmare, U. V.; Sood, A. K. Symmetry-Dependent Phonon Renormalization in Monolayer MoS₂ Transistor. *Phys. Rev. B* **2012**, *85*, 161403.
- (60) Grimme, S.; Antony, J.; Ehrlich, S.; Krieg, H. A Consistent and Accurate Ab Initio Parametrization of Density Functional Dispersion Correction (DFT-D) for the 94 Elements H-Pu. *J. Chem. Phys.* **2010**, *132*, 154104.

- (61) Perdew, J. P.; Zunger, A. Self-Interaction Correction to Density-Functional Approximations for Many-Electron Systems. *Phys. Rev. B* **1981**, *23*, 5048.
- (62) Atomistix ToolKit, v.13.8.0; QuantumWise A/S; <http://www.quantumwise.com/>.
- (63) Mulliken, R. S. Electronic Population Analysis on LCAO[Single Bond]MO Molecular Wave Functions. I. *J. Chem. Phys.* **1955**, *23*, 1833–1840.
- (64) Kang, J.; Sarkar, D.; Liu, W.; Jena, D.; Banerjee, K. A Computational Study of Metal-Contacts to beyond-Graphene 2D Semiconductor Materials. *IEEE Int. Electron Devices Meet.* **2012**, 17.4.1–17.4.4.
- (65) Kang, J.; Liu, W.; Sarkar, D.; Jena, D.; Banerjee, K. Computational Study of Metal Contacts to Monolayer Transition-Metal Dichalcogenide Semiconductors. *Phys. Rev. X* **2014**, *4*, 031005.
- (66) Sarkar, D.; Banerjee, K. Proposal for Tunnel-Field-Effect-Transistor as Ultra-Sensitive and Label-Free Biosensors. *Appl. Phys. Lett.* **2012**, *100*, 143108.
- (67) Sarkar, D.; Banerjee, K. *Fundamental Limitations of Conventional-FET Biosensors: Quantum-Mechanical-Tunneling to the Rescue*. 70th Device Research Conference; IEEE, Bellingham, WA, 2012; pp 83–84.
- (68) Sarkar, D.; Gossner, H.; Hansch, W.; Banerjee, K. Tunnel-Field-Effect-Transistor Based Gas-Sensor: Introducing Gas Detection with a Quantum-Mechanical Transducer. *Appl. Phys. Lett.* **2013**, *102*, 023110.
- (69) Sarkar, D.; Gossner, H.; Hansch, W.; Banerjee, K. Impact-Ionization Field-Effect-Transistor Based Biosensors for Ultra-Sensitive Detection of Biomolecules. *Appl. Phys. Lett.* **2013**, *102*, 203110.
- (70) Miremadi, B. K.; Singh, R. C.; Morrison, S. R.; Colbow, K. A Highly Sensitive and Selective Hydrogen Gas Sensor from Thick Oriented Films of MoS₂. *Appl. Phys. A: Mater. Sci. Process* **1996**, *63*, 271–275.